HHS Public Access

Author manuscript

Clin Neurophysiol. Author manuscript; available in PMC 2023 January 18.

Published in final edited form as:

Clin Neurophysiol. 2022 November ; 143: 97–106. doi:10.1016/j.clinph.2022.08.023.

Automated EEG-based prediction of delayed cerebral ischemia after subarachnoid hemorrhage

Wei-Long Zheng[a,e,1], **Jennifer A. Kim**[b,1], **Jonathan Elmer**[c], **Sahar F. Zafar**[a], **Manohar Ghanta**[a], **Valdery Moura Junior**[a], **Aman Patel**[d], **Eric Rosenthal**[a], **M. Brandon Westover**[a,*]

[a]Department of Neurology, Massachusetts General Hospital, Boston, MA 02114, USA

[b]Department of Neurology, Yale University, New Haven, CT 06520, USA

[c]Department of Critical Care Medicine, University of Pittsburgh Medical Center, Pittsburgh, PA 15213, USA

[d]Department of Neurosurgery, Massachusetts General Hospital, Boston, MA 02114, USA

[e]Department of Computer Science and Engineering, Shanghai Jiao Tong University, Shanghai 200240, China

Abstract

Objective: Delayed cerebral ischemia (DCI) is a leading complication of aneurysmal subarachnoid hemorrhage (SAH) and electroencephalography (EEG) is increasingly used to evaluate DCI risk. Our goal is to develop an *automated* DCI prediction algorithm integrating multiple EEG features over time.

Methods: We assess 113 moderate to severe grade SAH patients to develop a machine learning model that predicts DCI risk using multiple EEG features.

Results: Multiple EEG features discriminate between DCI and non-DCI patients when aligned either to SAH time or to DCI onset. DCI and non-DCI patients have significant differences in alpha-delta ratio (0.08 vs 0.05, $p < 0.05$) and percent alpha variability (0.06 vs 0.04, $p < 0.05$), Shannon entropy ($p < 0.05$) and epileptiform discharge burden (205 vs 91 discharges per hour, $p < 0.05$) based on whole brain and vascular territory averaging. Our model improves predictions by emphasizing the most informative features at a given time with an area under the receiver-operator curve of 0.73, by day 5 after SAH and good calibration between 48–72 hours (calibration error 0.13).

Conclusions: Our proposed model obtains good performance in DCI prediction.

Significance: We leverage machine learning to enable rapid, automated, multi-featured EEG assessment and has the potential to increase the utility of EEG for DCI prediction.

* Corresponding author at: Department of Neurology, Massachusetts General Hospital, 55 Fruit St, Boston, MA 02114, USA. mwestover@mgh.harvard.edu (M. Brandon Westover).

[1]Co-first authors.

Declaration of Competing Interest

The authors declare that they have no known competing financial interests or personal relationships that could have appeared to influence the work reported in this paper.

Keywords

EEG; Subarachnoid hemorrhage; Delayed cerebral ischemia; Machine learning; Epileptiform discharges; Biomarkers

1. Introduction

Delayed cerebral ischemia (DCI) is a major cause of morbidity following aneurysmal subarachnoid hemorrhage (SAH) (Dupont et al., 2010; Rowland et al., 2012; Vergouwen et al., 2011). While vasospasm is the best known risk factor for DCI, emerging evidence suggests that several mechanisms contribute, including cortical spreading depolarization, impaired cerebral autoregulation, microcirculatory dysfunction, neuroinflammation and microthrombosis (Budohoski et al., 2012; Carr et al., 2013; Dreier et al., 2009; Vergouwen et al., 2008). Given the multiple factors leading to DCI, modalities based on surveillance for vasospasm alone are insufficient to characterize risk for DCI. Continuous EEG (cEEG) has emerged as a diagnostic tool with potential for broader DCI detection (Claassen et al., 2004a; Rosenthal et al., 2018; Vespa et al., 1997).

Several types of cEEG changes have been associated with increased risk of DCI. Relative alpha variability, or percent alpha variability (PAV), describes the degree of alpha power (8–13 Hz) fluctuation over time. Decreasing variability suggests impending DCI (Vespa et al., 1997). Reduction of the ratio of power in the alpha vs delta frequency bands, or alpha-delta ratio (ADR), may also precede clinical DCI events (Claassen et al., 2004a). Absolute power bands have also been explored with mixed results (Claassen et al., 2004a; Gollwitzer et al., 2015; Rots et al., 2016). Most recently, appearance of epileptiform abnormalities was found to be correlated with increased DCI risk (Kim et al., 2017; Rosenthal et al., 2018). These results support EEG as a promising tool for early detection of impending DCI.

However, these studies required manual EEG review by a neurophysiologist and/or manual identification of artifact-free EEG segments. Such resource and time intensive approaches restrict the implementation of cEEG as a DCI prediction tool. An *automated* approach is essential to scaling up the use of cEEG for DCI detection. Early attempts at automation performed poorly, but only basic signal processing methods were employed (Wickering et al., 2016).

In this study, we develop an algorithm for DCI detection that improves upon performance of prior automated models. To accomplish this, we combined a weighted artifact detection calculation with multiple auto-calculated quantitative cEEG features using a machine learning approach to predict the development of DCI after subarachnoid hemorrhage.

2. Methods

Study population:

We included patients treated at a single academic medical center between September 2011 and January 2015. Inclusion criteria were: age ≥ 18 years; Hunt Hess 4–5 or Fisher grade 3 SAH; cEEG data 24 hours; and cEEG monitoring was not discontinued more than ≥ 24

hours before any clinically diagnosed DCI events. We excluded patients who developed status epilepticus (convulsive or non-convulsive), because mechanisms of secondary brain injury in frank status epilepticus may be distinct. We perform cEEG monitoring for ischemia detection as part of routine clinical care, day 2–10 after SAH, unless otherwise indicated. The MGH institutional review board approved this study (#2013P001024).

DCI classification:

We defined DCI according to an international consensus definition(Vergouwen et al., 2010) as either (1) new focal neurologic deficits and/or decrease in the Glasgow Coma Scale of at least 2 points, ≥one hour, not explained by other causes (e.g. procedural complications, sedation, intracranial hypertension, hydrocephalus, systemic abnormalities) based on clinical assessment, imaging or laboratory data, or (2) the presence of cerebral infarction on CT or MRI imaging of the brain, that was not present on any neuroimaging done within the first 48 hours following early aneurysm occlusion, and not attributable to other causes such as surgical clipping or endovascular treatment.

We adjudicated development of DCI by: (1) prospective daily structured research coordinator interview with the clinical team, (2) independent medical record review by three of the authors (ESR, MBW, SFZ) blinded to cEEG findings, (3) consensus adjudication by the same three authors in cases of uncertainty or disagreement.

If a patient experienced DCI at any point during hospitalization, this was documented, even if after cessation of cEEG recording. Patients with DCI events occurring > 24 hours after discontinuation of cEEG monitoring were excluded (see Study Population above).

Computer code.

We performed all analyses using Matlab (Natick, MA) and Python. All code and data needed to reproduce the figures are available at Github (https://github.com/mghcdac/SAH__DCI_Prediction_EEG).

Data preprocessing.

We recorded EEG data with 19 monopolar channels according to the international 10–20 system. We filtered raw EEG signals with a band-pass filter between 0.5 Hz and 30 Hz and a notch filter of 60 Hz. EEGs were re-sampled to 200 Hz and rereferenced to create 18 bipolar channels (Fp1-F7, F7-T3, T3-T5, T5-O1, Fp2-F8, F8-T4, T4-T6, T6-O2, Fp1-F3, F3-C3, C3-P3, P3-O1, Fp2-F4, F4-C4, C4-P4, P4-O2, Fz-Cz, Cz-Pz). To reduce contributions of noise and artifacts, we developed a weighting approach based on signal quality of each epoch. We automatically identified the following typical types of artifacts within each 5-s epoch: 1) abnormally high amplitude values above 500 μV; 2) small standard deviation of the signal (<0.2 μV) for more than 2 s; 3) overly fast amplitude change with more than 900 μV within 0.1 s; 4) staircase-like spectral patterns (commonly caused by ICU electrical equipment such as cooling blankets or pumps). A signal quality score was calculated as the percentage of clean 5-s epochs within each 5-min EEG segment. The quality scores within each one-hour time interval were normalized to the range 0 to 1 such that the EEG

features calculated in the 5-min segments with the least amount of artifact were weighted more heavily than those 5-min segments with more artifact each hour.

Feature extraction.

For every 5-min epoch, we extracted 9 EEG features: ED burden, Shannon entropy, delta (0.5–4 Hz), theta (4–7 Hz), alpha (8–15 Hz), beta (16–31 Hz), total (0.5–15 Hz) band power, alpha/delta ratio (ADR), and percent alpha variability (PAV). We used commercial spike detection software(Scheuer et al., 2017) to identify epileptiform discharges (ED). We computed ED burden as number of discharges (sporadic or periodic) detected per hour. Shannon entropy measures the information content of a signal. We calculated spectral features in the alpha, delta, theta, beta and total power bands using the short time Fourier transform (STFT) with Hamming windows. ADR and PAV were calculated by the ratio of alpha to delta band power, and the ratio of alpha to total band power, respectively.

We assessed spatial information by grouping the calculated spectral features into six regions (a.k.a., “vascular territory features”), based roughly on the territories of the anterior cerebral artery (ACA), middle cerebral artery (MCA), and posterior cerebral artery (PCA), respectively, of each hemisphere. The bipolar channels of ACA, MCA, and PCA were (Left: Fp1-F7, Fp1-F3; Right: Fp2-F8, Fp2-F4), (Left: F7-T3, T3-T5, F3-C3, C3-P3; Right: F8-T4, T4-T6, F4-C4, C4-P4), and (Left: T5-O1, P3-O1; Right: T6-O2, P4-O2), respectively. To calculate asymmetry features, we subtracted features of the same vascular territories between left and right hemispheres and used the absolute value of the difference. We calculated vascular territory features and corresponding asymmetry features on all EEG features except ED burden. To leverage trends in ED burden, ADR and PAV over time, we additively accumulated these features each hour. Missing values were imputed with linear interpolation across time. Values below the 10 percentile or above the 90th percentile were set to the 10th or 90th percentile values, respectively, to reduce the influence of outliers. We first aligned all these features to the time of SAH onset and then aligned them to the time of DCI onset when comparing between DCI and no DCI patient groups. To assess feature discrimination aligned to the time of DCI, we used previously published methods (Kim et al., 2022). Briefly, to generate comparisons relative to the day of DCI between DCI and non-DCI patients, we first identified each DCI patient and found their cEEG recording time and DCI onset time. Then we searched all non-DCI patients to determine who had recordings during that same time frame. This process was repeated iteratively for each DCI patient, such that multiple controls were matched to each DCI patient and each non-DCI patient could be re-used to match multiple DCI patients. Feature discrimination was then calculated between DCI and non-DCI patients based on this DCI-aligned time course.

Model development.

We developed multiple Random Forest (RF) classifiers to predict DCI every-six hours after onset of SAH. The individual features calculated above, and their combinations, were used as inputs to each classifier. Discrimination was analyzed with features derived from whole-brain averages, by hemisphere as well as from separate vascular territories. The optimal number of trees in the Random Forest was determined using cross validation and set to 50. For each six-hour interval after SAH we built a model identifying the hour of data

at which each feature was best discriminated between DCI and non-DCI groups during that time interval. This time point is defined as the time with the largest absolute difference of mean values divided by the square of the product of standard deviations of the two groups. This yielded a new model for each six-hour interval. This method allowed us to determine if there was a particular 6-hour interval after SAH onset that performed best at DCI prediction.

Since EEG features evolve over time, we also developed a time-sensitive prediction model to leverage past temporal information, a.k.a, our “max carry forward model”. To leverage information about past EEG time windows, we took this series of six-hour models and sequentially averaged the output of each model to generate the current predicted probability based on time after SAH onset. The framework of our study is illustrated in Fig. 1.

Performance evaluation.

Area under the receiver operating characteristic curve (AUC-ROC) and calibration error (absolute deviation from diagonal line) were used as performance metrics for each six-hour interval. Calibration error compares predicted probabilities with the observed event frequencies. If a model is well-calibrated, the output probability value matches the actual probability that the patient has the event. We chose to use AUC-ROC and calibration error to directly compare performance across models over time, since the optimal threshold for calculating sensitivity and specificity may vary for each model.

We used cross validation methods to evaluate our model performance. We performed fivefold cross validation for each 6-h model, by randomly partitioning the data into 5 folds, where 4 folds were used to train model parameters and the remaining 1-fold was used for model evaluation. Fivefold cross validation was repeated 20 times and performance metrics were reported as averages over all rounds of cross validation, together with 95 % confidence intervals. To evaluate feature discrimination, model performance was evaluated at different time intervals irrespective of the time of DCI occurrence. We also evaluated model performance accounting for DCI onset times. A good predictive model should identify DCI prior to onset, to serve as an alarm in clinical monitoring. Predictions of DCI were defined as true positive if made before DCI onset and false negative if DCI prediction was made after the actual DCI time.

Statistical analysis.

95 % confidence intervals and p values were reported to summarize statistical differences between the two groups. We used a significance threshold of 0.05. The 95 % confidence intervals on model performance were calculated by bootstrapping. By repeating the sampling and evaluation 5000 times, we obtained a bootstrap distribution over each performance metric and report the 2.5 and 97.5 percentiles as the 95 % confidence intervals.

3. Results

Overall, 107 patients met inclusion criteria, of whom 58 (54 %) developed DCI after a median of 6.45 days [IQR 4.75–9.42]. Mean age of the total cohort is 56 ± 14 years old and 79 patients (70 %) were female.

3.1. EEG feature discrimination of DCI aligned to SAH

We first analyzed the evolution of ED burden, ADR and PAV after SAH onset (Fig. 2a). DCI patients consistently had higher ED burden (mean = 206 ED/h, 95 % CI:197–215) vs non-DCI patients (91 ED/h, 95 % CI:86–96), with significant differences from 70–178 h after SAH (t-test, $p < 0.05$). Early ADR and PAV reductions were most strongly associated with DCI. Mean ADR of controls and DCI patients in the first five days after SAH were 0.086 (0.082–0.090) and 0.053 (95 % CI:0.051–0.056), respectively, with a significant difference from 29–129 h (t-test, $p < 0.05$). Mean PAV for control and DCI groups were 0.067 (95 % CI: 0.065–0.069) versus 0.046 (95 % CI: 0.045–0.048), with significant differences at 28–128 h (t-test, $p < 0.05$). To leverage temporal relationships, we summed features over time. The cumulative trends of ED burden, ADR and PAV all significantly differentiated DCI and control group (Fig. 2b).

Assessing features based on vascular territories and hemisphere asymmetry enhanced discrimination. For example, whole-brain averaged total power only discriminated late after SAH (Fig. 3a) but vascular territories showed significant differences by day 5 (Fig. 3b; t-test, $p < 0.05$). DCI discrimination was regionally enhanced for ADR, PAV, delta power and alpha power. Feature discrimination in the MCA territory was better than other territories for most features. Hemispheric asymmetry of Shannon entropy (EEG complexity) in DCI patients was significantly higher in the MCA region 2–3 days after SAH (Fig. 3c, t-test, $p < 0.05$). DCI patients also had larger hemispheric differences in theta and alpha power.

3.2. Combining selected EEG features improves discrimination of DCI

We evaluated model performance using different feature combinations. Fig. 4a shows the mean AUC per 6-h time interval using whole-brain, vascular territory, hemispheric asymmetry and combinations of features (ED burden was always included). We found whole-brain and vascular territory features achieved better performance early after SAH with mean AUC of 0.65, while asymmetry features performed better at later timepoints. Combining all features did not improve model performance. Therefore, we selected features strongly associated with DCI based on curve separation between the two groups, which improved model performance (Fig. 4b). The selected features were ED burden, ADR and PAV of whole-brain and vascular territory, alpha band in PCA, total band and delta band in ACA, asymmetry alpha band in MCA and PCA, asymmetry delta band in MCA, asymmetry Shannon entropy in ACA and MCA, asymmetry theta and total bands in MCA, and cumulative features. This model achieved higher performance on day 4–5 after SAH (AUC 0.67), with best AUCs 0.7–0.75 on day 9–10 after SAH. While the mean values of the features do indeed show good separation, these are group effects: i.e. the features are different on average in patients with vs without eventual DCI. The feature value differences between two groups were not always large in individual patients. The AUC measures the ability of a classifier to distinguish between individual patients with vs without DCI. Since the best performance of this initial model was at later timepoints, and thereby less clinically useful, we modified our methods to introduce a time-sensitive machine learning model to improve early model prediction (i.e., max carry forward method).

3.3. Differences in EEG features precede DCI time, when aligned to that event

To assess feature evolution in relation to DCI onset, we aligned EEG features according to DCI times (Fig. 5a). We matched all control patients who had EEG recordings during the same timeframe as each DCI patient prior to their DCI onset. This prevented confounding of any time dependence of EEG features seen across both groups (see Methods). Control patients could be used multiple times if their EEG recording timeframe matched multiple DCI patients. This resulted in matching 1050 control patient segments to 58 DCI patients. DCI patients had increasing ED burden and theta power 5 days prior while ADR and PAV differences were observed 3 days prior to DCI. Shannon entropy showed higher EEG complexity (more fast waves) 4 days prior to DCI. On the day of DCI (day = 0), only ED burden, ADR, PAV and alpha power showed significant differences. The difference of cumulative trends in ED burden increases over time, while ADR and PAV differences show mainly early divergence (Fig. 5b). We also assessed feature evolution based on vascular territories and hemisphere asymmetry which showed feature discrimination for DCI patients in ADR, PAV, Shannon entropy, theta and alpha power ($p < 0.05$).

DCI prediction performance over time aligned with DCI. Mean AUC values and standard deviations of spectral whole-brain, vascular territory, asymmetry features and their combination were 0.70 ± 0.06, 0.81 ± 0.05, 0.71 ± 0.04, and 0.80 ± 0.04, respectively (Fig. 6). Vascular territory-based features performed best. Combining *all* features, including ED burden and cumulative features, improved model performance when aligned to DCI onset (AUC 0.85 ± 0.05 up to two days prior to DCI onset). Prediction performance aligned to DCI was higher than models aligned to SAH.

3.4. Improved early model performance using a max carry forward model after SAH

To further improve early prediction after SAH, we propose a new time-sensitive “max carry forward” model which averages the prediction probabilities of successive models at six-hour intervals which account for the best feature discrimination within each interval (see Methods; Fig. 7a). We compared the performance of this model with the baseline model (Fig. 4), which was trained and tested independently at each time interval. The max-carry-forward model improved early identification of DCI patients, and progressively improved. The mean prediction AUC increased from 0.61 (day 2; 95 % CI: 0.57–0.65) to 0.73 (day 5; 95 % CI: 0.69–0.77) after SAH. The sensitivity/specificity improved from on 57 %/64 % day 2 to 72 %/65 % on day 5 after SAH. Based on the ROC curve on day 5, an FNR threshold of 30 % results in an FPR of 31 %. The mean AUC values between day 2–10 after SAH were 0.70 (95 % CI: 0.62–0.73) for the max carry forward model vs 0.64 (95 % CI: 0.55–0.74) for the baseline model. Thus, this max-carry-forward model significantly improves the performance (t-test, $p < 0.01$). We also compared model performance with and without artifact detection in Fig. 7a. The model with artifact detection performed much better than without artifact, demonstrating a consistent performance gap between these methods. These results support the utility of including an artifact detection method in the framework.

Generally, prediction probabilities of DCI are higher in DCI than non-DCI patients. In Fig. 7a, we evaluated the model performance at different time intervals regardless of DCI time.

Fig. 7b demonstrates the prediction probabilities generated by the max carry forward model over time after SAH for each patient. However, in practice a good model must provide an accurate alarm of DCI *prior* to DCI onset. Therefore, we evaluated the model performance accounting for true positives (aka., classified as positive *prior* to DCI) vs false negatives (a.k.a, classified positively *after* the DCI event) (Fig. 7c). When the features were aligned to DCI, The mean AUC value was 0.66 (95 % CI: 0.56–0.76). The model's sensitivity was 41 % for a specificity threshold of 80 %. The model's specificity was 40 % for a sensitivity threshold of 80 %.

Model calibration, a measure of systematic errors of over- or under-prediction, was evaluated to assess suitability of the model's prediction probability as a DCI risk score for clinical applications. We compared calibration curves at different time intervals and calculated calibration errors to quantify performance (Fig. 7d–e). Calibration error was defined as the mean absolute deviation from the diagonal line, which represents perfect calibration (a.k.a., no systematic errors of over- or under-prediction; see Methods). The calibration errors were 0.16 at 48 h and 0.13 for all other time point (54 h, 60 h, 66 h, and 72 h). Assessing risk calibration for our DCI aligned model, we obtained a calibration error of 0.07 at 18–12 h prior to DCI (Fig. 7e). Thus, all models had good calibration.

4. Discussion

In this study, we demonstrate that an automated algorithm combining select EEG features can predict DCI. Our model bypasses the need for manual EEG review by incorporating weighted artifact rejection methods followed by automated calculations of EEG spectral features in a large patient cohort. In addition to exploring several quantitative EEG (qEEG) features simultaneously, we assessed the contributions of incorporating both spatial and temporal features. We showed that these features discriminate DCI from non-DCI patients both when aligned to time of SAH or to the time of onset of DCI. Finally, we developed a time-sensitive model which predicts DCI with acceptable performance early after SAH with low calibration error. Since the EEG features evolved over time, the time-sensitive "max carry forward" model was trained and evaluated for each 6 h time interval. The max-carry-forward model significantly improved the performance in comparison with the baseline method.

We explored both new and established qEEG features in assessing DCI risk in our cohort. Our results confirm ADR and PAV decreases in DCI patients compared to controls, confirming prior work which used curated EEG data (Claassen et al., 2004a; Rosenthal et al., 2018; Vespa et al., 1997). The (sensitivity, specificity) of our automatically computed ADR and PAV features were (0.69, 0.67) at 60 h after SAH and (0.76, 0.59) at 54 h after SAH, respectively, using univariate analysis. This is lower than a recent meta-analysis which reported ADR with a sensitivity and specificity of 0.84 and 0.74 (Yu et al., 2019). However, the five studies comprising this meta-analysis reported sensitivities from 0.33–1.0 and specificities from 0.34 to 0.9 (Claassen et al., 2004a; Gollwitzer et al., 2015; Rosenthal et al., 2018; Rots et al., 2016; Wickering et al., 2016). For studies with sample sizes ≥ 50 patients, sensitivity and specificity were 0.76 and 0.67 respectively,(Yu et al., 2019) similar to our results. Thus, while individual spectral features at whole-brain, hemispheric

and vascular distributions show reasonable predictive value for DCI, these data suggest that single feature predictive performance is limited.

By assessing features at both a whole-brain and regional level, we enhanced the discriminatory utility of each feature. The concept of separating EEG signals based on regional territory and/or hemisphere asymmetry is supported based on pathophysiology and prior studies (Claassen et al., 2004a; Rosenthal et al., 2018; Vespa et al., 1997). Doing this, we found that MCA territory features have better feature discrimination than other territories. One explanation is that the MCA territory accounts for a large portion of the cortical surface and thus, changes in here are more reliably detected on EEG. Another possibility is that DCI events based on motor or language changes in exam, functions mainly associated with the MCA territory, are more obvious. Relatedly, we found that left MCA feature discrimination was better than the right MCA, suggesting left MCA symptoms are more easily recognized than right MCA symptoms. These observations highlight the importance of incorporating spatial vascular information into prediction.

Our final goal was to develop a time-sensitive model compared to prior time-independent models. We first used simple additive cumulation curves for ED burden, ADR and PAV and independent features. This improved model performance, but mainly at later timepoints in the DCI window. Then, we implemented a max-carry forward method, described in the Methods section, which resulted in better performance *early* within the DCI window improving clinical applicability. We found that calibration errors at all 6-hour windows of the model were low, suggesting that the model accurately predicts low, moderate and high probabilities of DCI. This model is the first to utilize historical EEG information to improve DCI prediction. Importantly, because our clinical EEG monitoring protocol focused on moderate to high-grade SAH, our EEG based model helps *further stratify* patient risk amongst those who would otherwise be considered to have equally elevated risk for DCI based on clinical Fisher(3–4) or VASOGRADE(De Oliveira Manoel et al., 2015)(yellow, red) scales alone.

A major limitation of prior studies was that EEG data processing was not automated, requiring manual selection and calculations of EEG segments (Claassen et al., 2004b; Vespa et al., 1997). Our groups prior attempt to automate calculations of these features without a priori segment selection or artifact reduction yielded poor DCI prediction results (Wickering et al., 2016). Our new approach here utilized a method to more heavily weight the contribution of EEG segments that were relatively artifact free, followed by automated calculations of multiple qEEG features of those weighted EEG segments in a large patient sample, thereby avoiding the burden of manual review. In Fig. 7a, weighting the EEG features by the signal quality score reduced the influence of different artifacts introduced in EEG recordings and improved model performance. Therefore, our automated method can leverage more continuous EEG data for DCI detection without the high-cost of manual labeling. This weighted artifact reduction, in combination with spatially and temporally augmented features, provided us with a final model which improves upon prior single-feature, manually-segmented EEG algorithms. Alternative artifact detection and removal approaches may be worth pursuing in future research.

Our work has some important limitations. First, while we calculated features and test our algorithm in a larger patient sample size than most prior studies, the sample size is still limited and would be best validated in a larger multi-institutional cohort, especially to assess performance on an independent test set, rather than relying on cross-validation methods. Our sample size also limited the machine learning methods we could test. An increased patient sample would allow us to explore more sophisticated time-sensitive models such as long-short term memory (LSTM) networks, a type of deep-learning recurrent neural network. While we represented spatial differences by calculating asymmetry and vascular region features, patients were not divided based upon symptomatology. Future work to explore whether spatial discrimination is enhanced based on clinical symptoms would be important, but also requires a larger cohort. While our data hints at the clinical plausibility for differences in laterality observed for some features, these observations could be a consequence of sampling error and require validation. ED burden incorporated in our model, but no other waveform analysis was conducted. Future studies should explore ED features beyond burden and quantify other interictal patterns. Finally, a model which incorporates multimodal information, such as TCDs, radiologic imaging or time invariant features like clinical demographics, might achieve better performance.

5. Conclusion

This work demonstrates an automated model for DCI prediction combining multiple EEG features. We incorporate spatial and temporal information to improve prediction performance. By eliminating the need for manual EEG review, our model enhances the potential for implementation of cEEG as a tool for DCI prediction more broadly.

Funding

JAK received funding from NINDS (R25N065743, K23NS112596–01A1), American Heart Association, Bee Foundation. JE received funding from NINDS (5K23NS097629). MBW received funding from Glenn Foundation for Medical Research, American Federation for Aging Research (Breakthroughs in Gerontology); the American Academy of Sleep Medicine Strategic Research Award; DoD Moberg ICU Solutions, Inc, subcontract and NIH (1R01NS102190, 1R01NS102574, 1R01NS107291, 1RF1AG064312). WLZ was supported by NIH (1R01NS102574). SFZ is supported by NIH (K23NS114201). ESR was supported by NIH (1K23NS105950).

References

Budohoski KP, Czosnyka M, Smielewski P, Kasprowicz M, Helmy A, Bulters D, et al. Impairment of cerebral autoregulation predicts delayed cerebral ischemia after subarachnoid hemorrhage: A prospective observational study. Stroke 2012;43(12):3230–7. [PubMed: 23150652]

Carr KR, Zuckerman SL, Mocco J. Inflammation, cerebral vasospasm, and evolving theories of delayed cerebral ischemia. Neurol Res Int 2013;2013. 10.1155/2013/506584.

Claassen J, Hirsch LJ, Kreiter KT, Du EY, Sander Connolly E, Emerson RG, et al. Quantitative continuous EEG for detecting delayed cerebral ischemia in patients with poor-grade subarachnoid hemorrhage. Clin Neurophysiol 2004a;115(12):2699–710. [PubMed: 15546778]

Claassen J, Mayer SA, Kowalski RG, Emerson RG, Hirsch LJ. Detection of electrographic seizures with continuous EEG monitoring in critically ill patients. Neurology 2004b;62:1743–8. 10.1212/01.WNL.0000125184.88797.62. [PubMed: 15159471]

Dreier JP, Major S, Manning A, Woitzik J, Drenckhahn C, Steinbrink J, et al. Cortical spreading ischaemia is a novel process involved in ischaemic damage in patients with aneurysmal subarachnoid haemorrhage. Brain 2009;132(7):1866–81. [PubMed: 19420089]

Dupont SA, Wijdicks EFM, Lanzino G, Rabinstein A, a.. Aneurysmal subarachnoid hemorrhage: An overview for the practicing neurologist. Semin Neurol 2010;30:545–54. 10.1055/s-0030-1268862. [PubMed: 21207347]

Gollwitzer S, Groemer T, Rampp S, Hagge M, Olmes D, Huttner HB, et al. Early prediction of delayed cerebral ischemia in subarachnoid hemorrhage based on quantitative EEG: A prospective study in adults. Clin Neurophysiol 2015;126(8):1514–23. [PubMed: 25500193]

Kim JA, Rosenthal ES, Biswal S, Zafar S, Shenoy AV, O'Connor KL, et al. Epileptiform abnormalities predict delayed cerebral ischemia in subarachnoid hemorrhage. Clin Neurophysiol 2017;128(6):1091–9. [PubMed: 28258936]

Kim JA, Zheng W-L, Elmer J, Jing J, Zafar SF, et al. High epileptiform discharge burden predicts delayed cerebral ischemia after subarachnoid hemorrhage. Clin Neurophysiol 2022;141:139–46. [PubMed: 33812771]

de Oliveira Manoel AL, Jaja BN, Germans MR, Yan H, Qian W, Kouzmina E, et al. The VASOGRADE: A Simple Grading Scale for Prediction of Delayed Cerebral Ischemia after Subarachnoid Hemorrhage. Stroke 2015;46(7):1826–31. [PubMed: 25977276]

Rosenthal ES, Biswal S, Zafar SF, O'Connor KL, Bechek S, Shenoy AV, et al. Continuous Electroencephalography Predicts Delayed Cerebral Ischemia after Subarachnoid Hemorrhage: A Prospective Study of Diagnostic Accuracy. Ann Neurol 2018;83(5):958–69. [PubMed: 29659050]

Rots ML, van Putten MJAM, Hoedemaekers CWE, Horn J. Continuous EEG Monitoring for Early Detection of Delayed Cerebral Ischemia in Subarachnoid Hemorrhage: A Pilot Study. Neurocrit Care 2016;24:207–16. 10.1007/s12028-015-0205-y. [PubMed: 26432793]

Rowland MJ, Hadjipavlou G, Kelly M, Westbrook J, Pattinson KTS. Delayed cerebral ischaemia after subarachnoid haemorrhage: looking beyond vasospasm. Br J Anaesth 2012;109:315–29. 10.1093/bja/aes264. [PubMed: 22879655]

Scheuer ML, Bagic A, Wilson SB. Spike detection: Inter-reader agreement and a statistical Turing test on a large data set. Clin Neurophysiol 2017;128:243–50. 10.1016/J.CLINPH.2016.11.005. [PubMed: 27913148]

Vergouwen MDI, Etminan N, Ilodigwe D, Macdonald RL. Lower incidence of cerebral infarction correlates with improved functional outcome after aneurysmal subarachnoid hemorrhage. J Cereb Blood Flow Metab 2011;31:1545–53. 10.1038/jcbfm.2011.56. [PubMed: 21505477]

Vergouwen MDI, Vermeulen M, Coert BA, Stroes ESG, Roos YBWEM. Microthrombosis after aneurysmal subarachnoid hemorrhage: An additional explanation for delayed cerebral ischemia. J Cereb Blood Flow Metab 2008;28:1761–70. 10.1038/jcbfm.2008.74. [PubMed: 18628782]

Vergouwen MDI, Vermeulen M, van Gijn J, Rinkel GJE, Wijdicks EF, Muizelaar JP, et al. Definition of delayed cerebral ischemia after aneurysmal subarachnoid hemorrhage as an outcome event in clinical trials and observational studies: proposal of a multidisciplinary research group. Stroke 2010;41(10):2391–5. [PubMed: 20798370]

Vespa PM, Nuwer MR, Juhász C, Alexander M, Nenov V, Martin N, Becker DP. Early detection of vasospasm after acute subarachnoid hemorrhage using continuous EEG ICU monitoring. Electroencephalogr Clin Neurophysiol 1997;103(6):607–15. [PubMed: 9546487]

Wickering E, Gaspard N, Zafar S, Moura VJ, Biswal S, Bechek S, et al. Automation of Classical QEEG Trending Methods for Early Detection of Delayed Cerebral Ischemia: More Work to Do. J Clin Neurophysiol 2016;33(3):227–34. [PubMed: 27258446]

Yu Z, Wen D, Zheng J, Guo R, Li H, You C, et al. Predictive Accuracy of Alpha-Delta Ratio on Quantitative Electroencephalography for Delayed Cerebral Ischemia in Patients with Aneurysmal Subarachnoid Hemorrhage: Meta-Analysis. World Neurosurg 2019;126. e510–6.

HIGHLIGHTS

- A number of EEG features have been shown to be predictive of delayed cerebral ischemia (DCI), but a continuous assessment of multidimensional EEG features is lacking.
- Combining spectral and epileptiform discharge feature information, using automated calculations, allows for dynamic prediction of DCI.
- This dynamic multi-feature assessment increases the feasibility of implementing interventions in response to our EEG derived DCI risk probability.

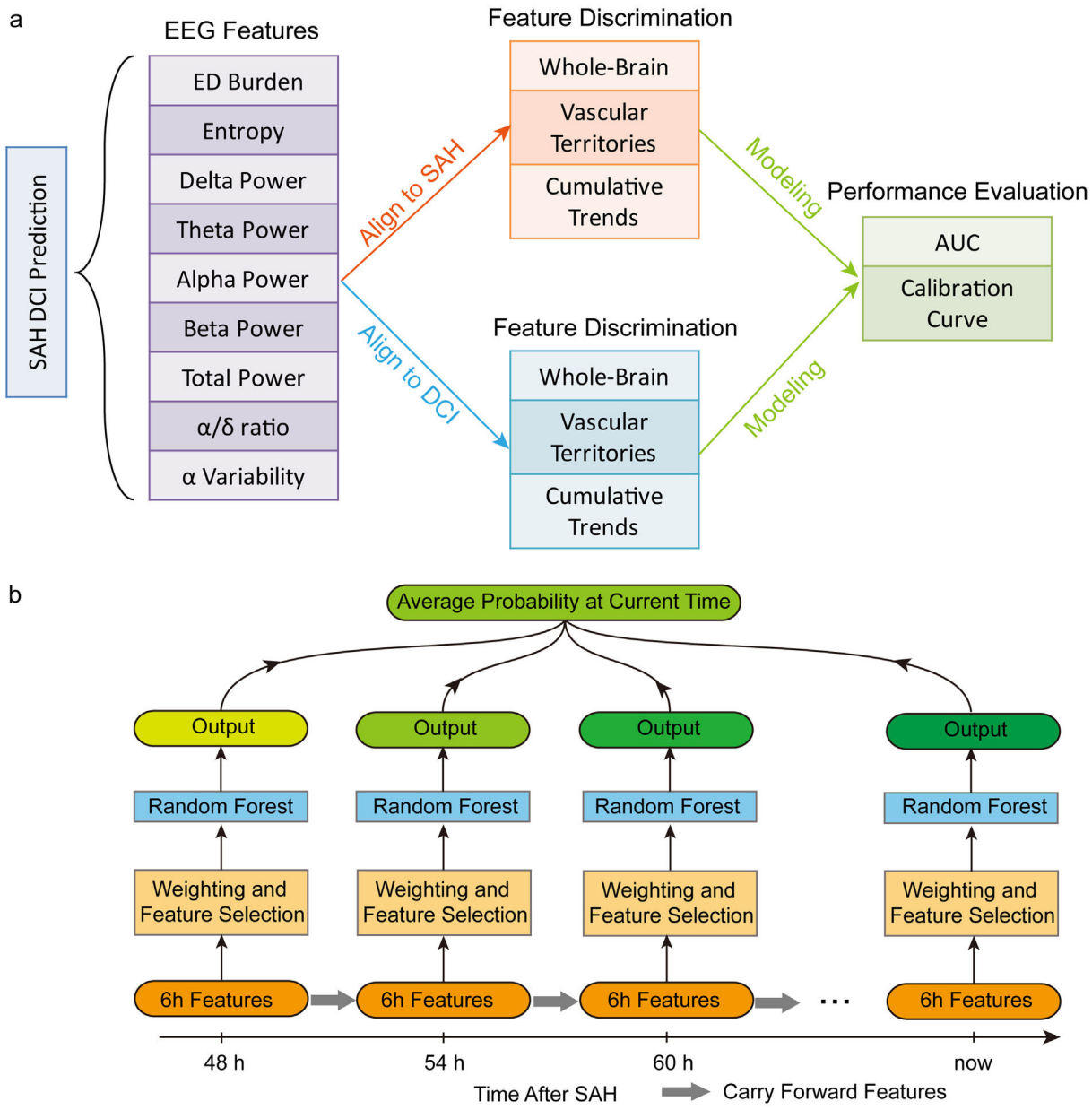

Fig. 1. Study Framework.

a, Nine quantitative EEG features (purple) were extracted and their feature were evaluated aligned to subarachnoid hemorrhage (SAH) onset (orange) and delayed cerebral ischemia (DCI) (blue) times, respectively. Feature discrimination was analyzed by the whole-brain average and vascular territories. Random forest models were built which cumulatively assessed these EEG features and their prediction performances (green). **b,** The prediction model carries forward the best features in the past and obtained evaluated performance using area under the receiver operating characteristic curve (AUC) and model calibration measures. Features were weighted based on artifact detection and selected based on feature discrimination of each 6 h time intervals (red and orange). A series of models were built

(blue) and the output was sequentially averaged (green) in each six-hour model to generate the current predicted probability.

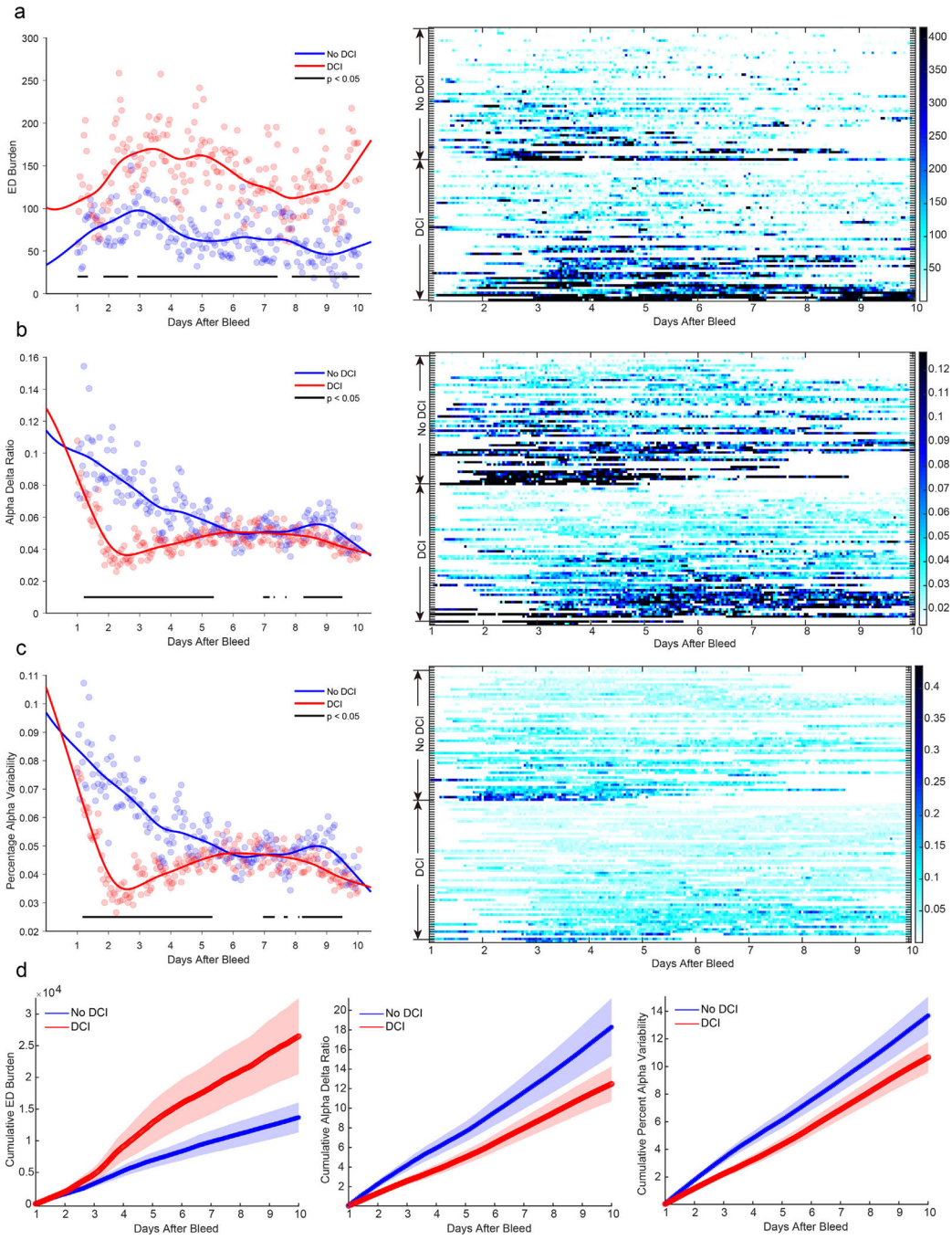

Fig. 2. Feature evolution over time and their cumulative trends after subarachnoid hemorrhage (SAH).

Fitted trends (left) were shown for: **a,** epileptiform discharges (ED) burden, **b,** alpha/delta ratio (ADR), **c,** percentage alpha variability (PAV) for delayed cerebral ischemia (DCI) (red) and no DCI (blue) patients, respectively. The bars below the mean curves indicate statistical significance (t-test, $p < 0.05$). Statistical significance was evaluated for each time intervals with four consecutive hours. The dots represent mean values per hour. On the right, swimmer plots show feature distributions over time, where each row shows the

corresponding feature evolution for one patient, where darker shading represents higher ED burden, ADR and PAV, respectively. ED burden, early ADR and PAV were strongly associated with DCI. **d,** The *cumulative* trends of ED burden, ADR, and PAV for DCI (red) and no DCI (blue) patients. The features were accumulated over time and missing data were linearly interpolated. The shaded areas represent standard errors.

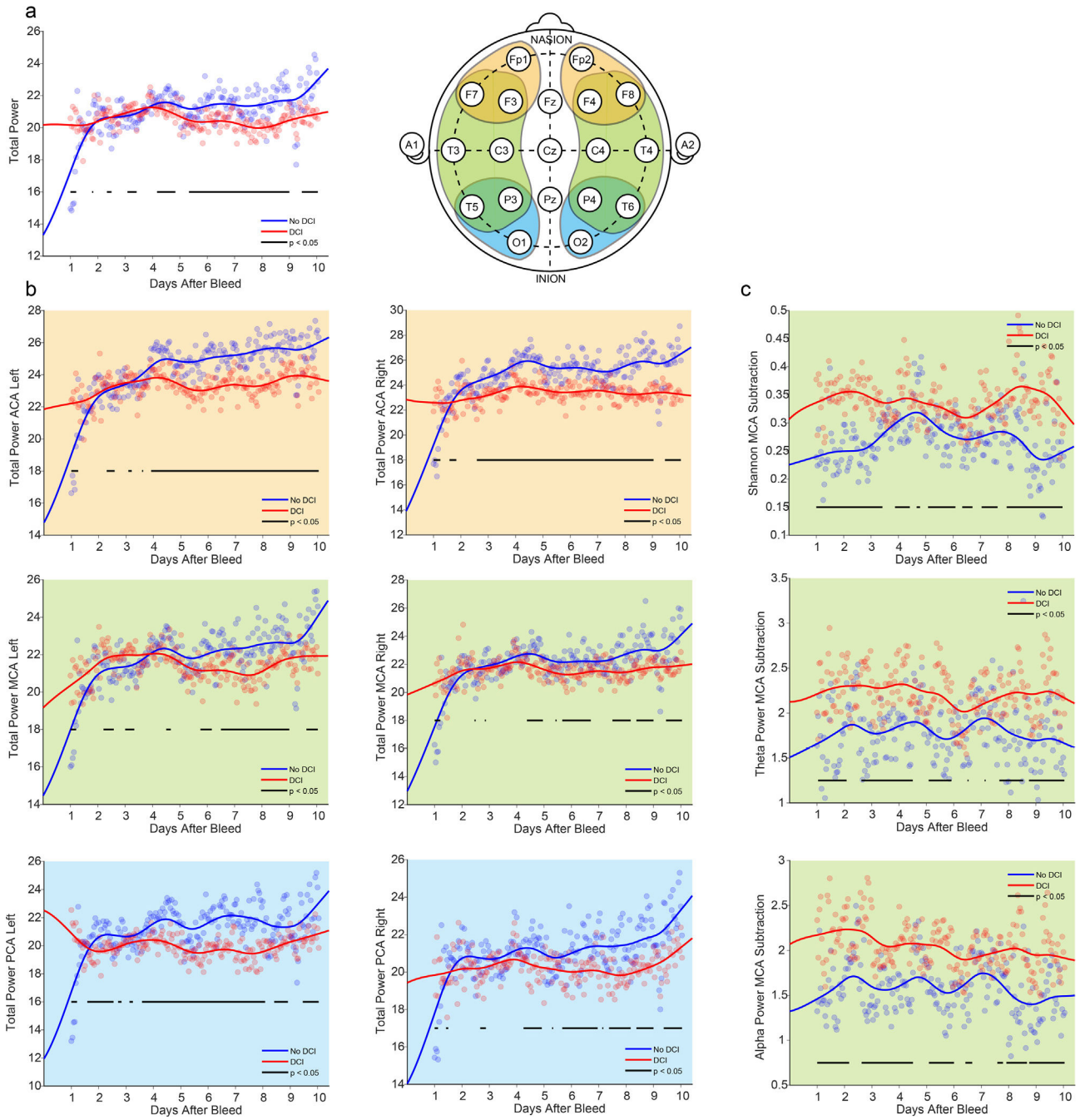

Fig. 3. Vascular territories and hemisphere asymmetry enhanced feature discrimination.

EEG electrodes were divided into their vascular territory representations (top right): anterior cerebral artery (ACA; orange), middle cerebral artery (MCA; green), and posterior cerebral artery (PCA; blue). Fitted trends of each feature are shown in delayed cerebral ischemia (DCI; red) and no DCI (blue) patients. **a,** total power based on the whole-brain averages, **b,** total power based on six vascular territories: ACA (orange background), MCA (green background), and PCA (blue background) of left and right hemispheres (from left to right). **c,** hemisphere asymmetry of MCA (green background) in Shannon entropy, theta power, and

alpha power (from top to bottom). EEG features were aligned to subarachnoid hemorrhage (SAH) time. The bars below the mean curves indicate statistical significance (t-test, $p < 0.05$). The statistical significance was evaluated for each four-hour time interval.

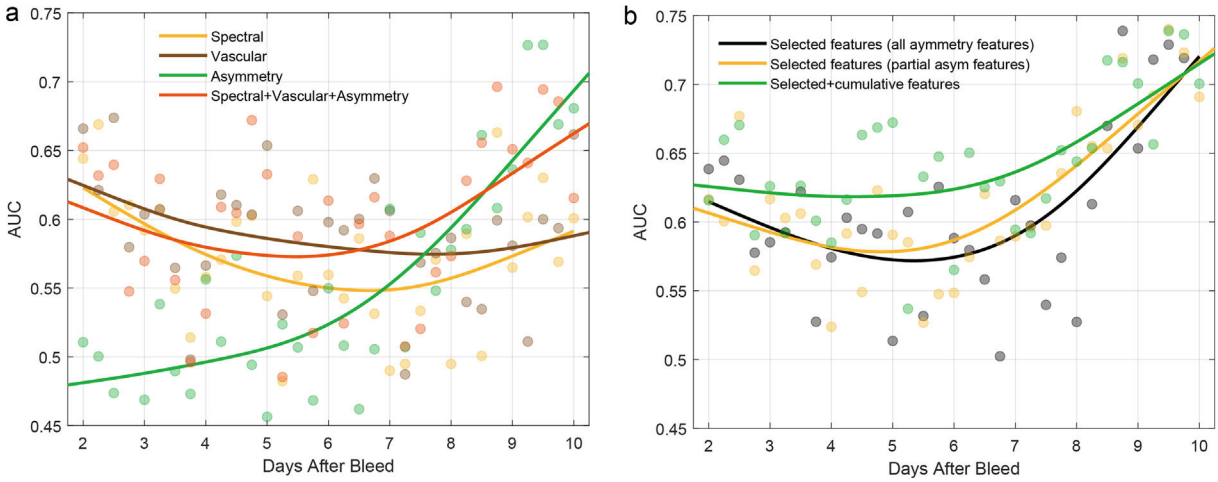

Fig. 4. Delayed cerebral ischemia (DCI) prediction performance over time using different features and feature combinations.

a, model performance of different EEG features and their combination. **b,** model performance of selected features and their combination with cumulative features. The model with the selected features performed best. The selected features were epileptiform discharges (ED) burden, alpha/delta ratio (ADR) and percentage alpha variability (PAV) based on whole-brain averages and all six vascular territories, alpha power based on left and right posterior cerebral arteries (PCAs), and total and delta power based on left and right anterior cerebral arteries (ACAs). The selected asymmetry features were alpha power of middle cerebral artery (MCA) and PCA, delta power of MCA, Shannon entropy of ACA and MCA, and theta and total power of MCA. The selected features and cumulative features achieved the best performance on 9–10 days after SAH. X axis is the time after subarachnoid hemorrhage (SAH) with a time step of 6 hours, and y axis is the mean area under the receiver operating characteristic curve (AUC) values in 5-fold cross-validation. The performance curves were smoothed using spline smoothing with a parameter of 0.001.

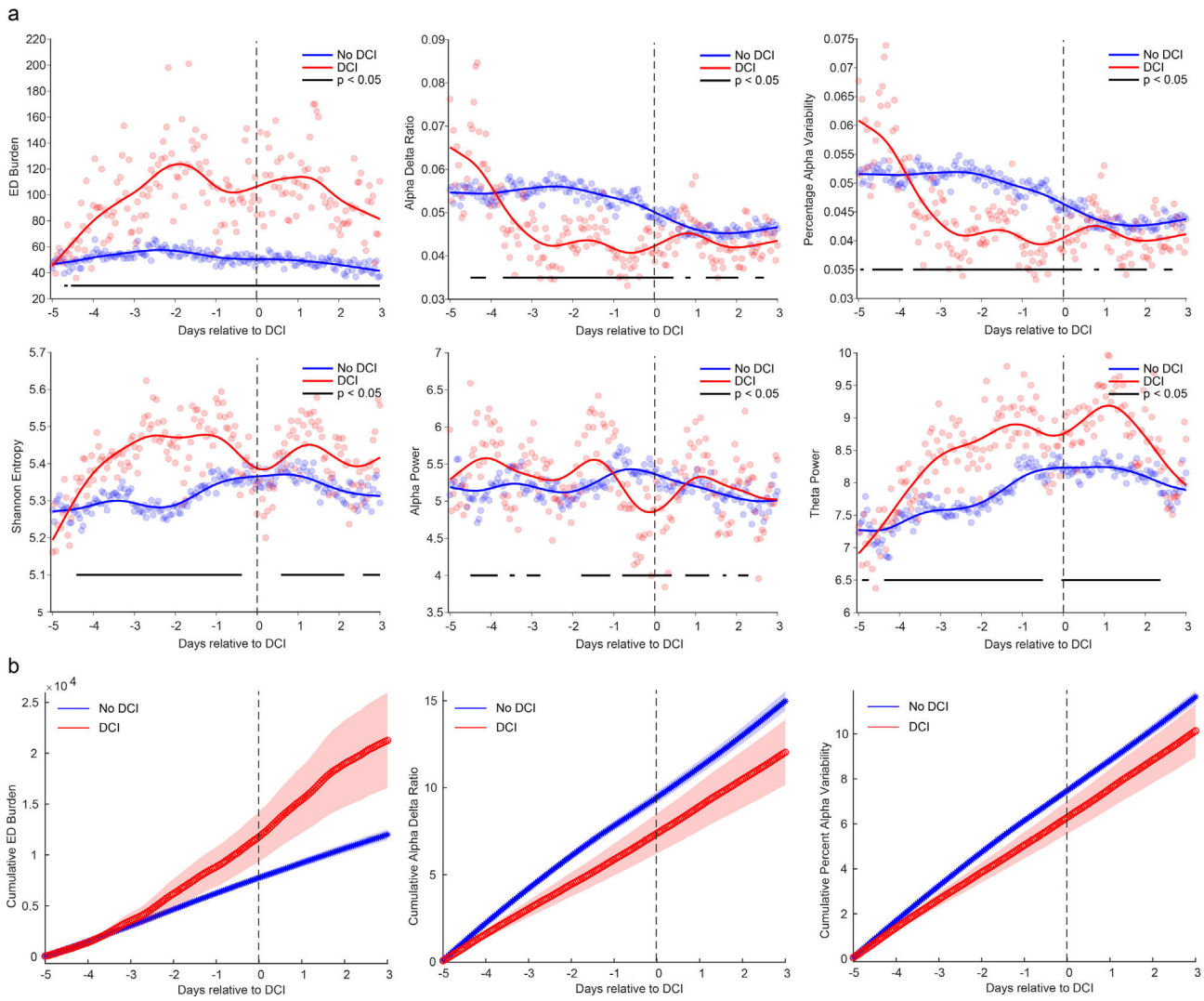

Fig. 5. Feature evolution over time and its cumulative trend aligned to delayed cerebral ischemia (DCI) time.

a, Fitted trends of EEG features aligned to DCI onset time. From top to bottom and from left to right, the features are epileptiform discharges (ED) burden, alpha/delta ratio, percentage of alpha variability, Shannon entropy, alpha power, and theta power. Red and blue colors indicate DCI and no DCI groups, respectively. Dashed lines indicate the DCI onset time. Bars above the mean curves indicate statistical significance (t-test, $p < 0.05$, longer than at least two consecutive hours). **b,** Cumulative trends of ED burden, alpha/delta ratio and percent alpha variability (left to right). The features were accumulated over time and missing data were linearly interpolated. The shaded areas represent standard errors.

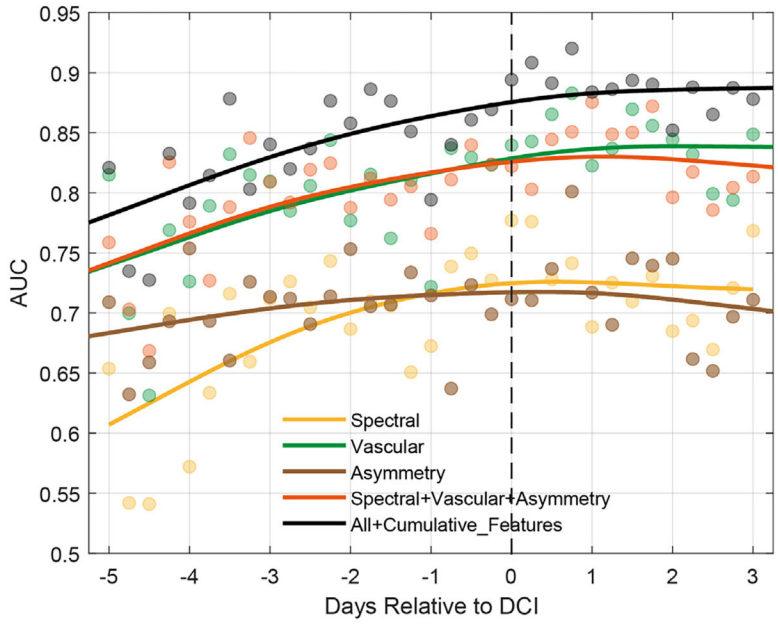

Fig. 6. Delayed cerebral ischemia (DCI) prediction performance over time, aligned to DCI, using EEG features and feature combination as inputs to classifiers.

Random forest models were built using spectral (orange), vascular (green) and hemisphere asymmetry (brown) measures of the EEG. A combination of all features (red) and all features plus cumulative features (black) were modeled showing that all features and cumulative features (black) had the best prediction performance. The performance curves were smoothed using spline smoothing with a parameter of 0.001.

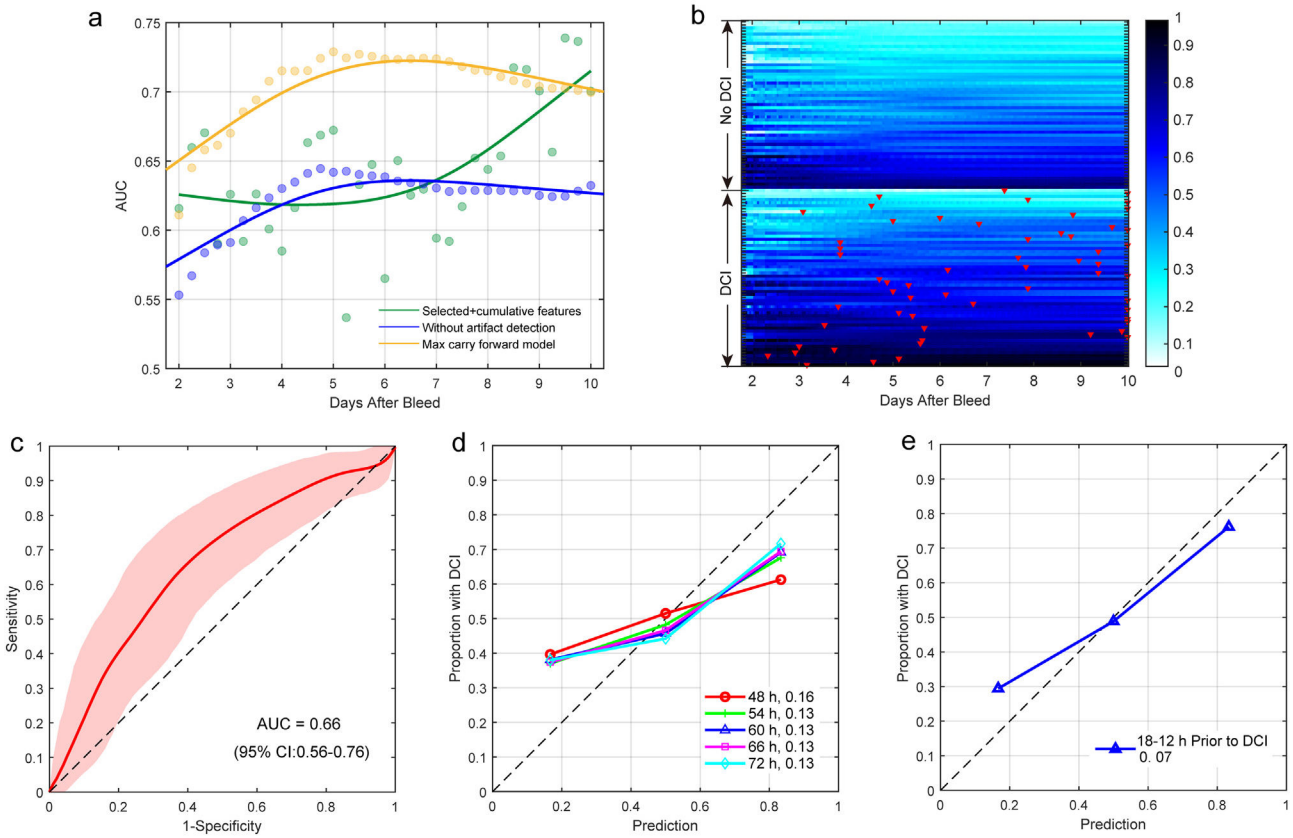

Fig. 7. Model performance of our max carry forward model.

a, Comparison of model performance with the baseline model (green) and the method without artifact detection (blue) vs our max carry forward model (yellow). Y-axis is the mean area under the receiver operating characteristic curve (AUCs) and x-axis is time after subarachnoid hemorrhage (SAH)). Performance curves were smoothed using spline smoothing with a parameter of 0.001. Dots represent the original AUC values at different time intervals. **b,** Swimmer plot of prediction probabilities over time for individual patients (one row per patient) using the max carry forward model. Red triangles represent delayed cerebral ischemia (DCI) events. DCI events later than 10 days after SAH were marked on day 10. **c,** receiver operating characteristic curve (ROC) curve of our max carry forward model considering only data up through the time of DCI to represent prediction performance prior to DCI onset. Shaded areas denote 95 % confidence intervals. **d,** Risk calibration curves of models at different time intervals after subarachnoid hemorrhage (SAH). The calibration errors are shown. **e,** Risk calibration curve of model at 18 h-12 h prior to DCI.